High-accuracy characterization of the edge radial electric field at ASDEX Upgrade

E. Viezzer[1], T. Pütterich[1], G. D. Conway[1], R. Dux[1], T. Happel[1], J. C. Fuchs[1], R. M. McDermott[1], F. Ryter[1], B. Sieglin[1], W. Suttrop[1], M. Willensdorfer[2], E. Wolfrum[1] and the ASDEX Upgrade Team[1]

[1] *Max-Planck-Institut für Plasmaphysik, EURATOM Association, Boltzmannstr. 2, 85748 Garching, Germany*

[2] *Institut für Angewandte Physik, Technische Universität Wien, Association EURATOM-ÖAW, 1040 Vienna, Austria*

E-mail: `Eleonora.Viezzer@ipp.mpg.de`

Abstract. The installation of a new poloidal charge exchange recombination spectroscopy (CXRS) diagnostic at ASDEX Upgrade (AUG) has enabled the determination of the radial electric field, E_r, using the radial force balance of impurity ions. E_r has been derived from charge exchange (CX) spectra measured on different impurity species, such as He^{2+}, B^{5+}, C^{6+} and Ne^{10+}. The resulting E_r profiles are found to be identical within the uncertainties regardless of the impurity species used, thus, demonstrating the validity of the diagnostic technique. The E_r profile has been compared to the main ion pressure gradient term, which is found to be the dominant contribution at the plasma edge, thus, supporting that the E_r well is created by the main ion species. The E_r profile has been measured in different confinement regimes including L-, I- and H-mode. The depth of the E_r well and the magnitude of the E_r shear are correlated with the ion pressure at the pedestal top. The temporal evolution of the measured CX profiles and the resulting E_r have been studied during an ELM cycle. At the ELM crash, the E_r minimum is less deep resulting in a reduction of the $\mathbf{E}\times\mathbf{B}$ shear. Within 2 ms after the ELM crash, the edge kinetic profiles have nearly recovered and the E_r well is observed to recover simultaneously. In high density type-I ELM mitigated H-mode plasmas, obtained via externally applied magnetic perturbations with toroidal mode number $n = 2$, no clear effect on E_r due to the magnetic perturbations has been observed.

PACS numbers: 52.55.Fa, 52.25.Vy, 52.30.-q, 52.70.-m

1. Introduction

The main baseline scenario for ITER is the H-mode [1], which is characterized by high energy and particle confinement times. H-mode plasmas exhibit an edge transport barrier (ETB) which causes a reduced level of heat and particle transport perpendicular to the magnetic field. The most accepted explanation for the ETB is the existence

of a strong shear in plasma flow perpendicular to the magnetic field caused by the radial electric field E_r. This $\mathbf{E}\times\mathbf{B}$ velocity shear is thought to be fundamental for edge turbulence suppression [2] thus, aiding the formation of the ETB and leading to the L-H transition. However, the origin and development of E_r is still not fully understood although the existence of an E_r well at the plasma edge is ubiquitous to toroidal magnetic confinement devices such as ASDEX Upgrade [3, 4], DIII-D [5], Alcator C-Mod [6], JET [7], JT-60U [8], TFTR [9], TEXTOR [10], MAST [11], NSTX [12], LHD [13], W7-AS [14], TJ-II [15] and RFX [16]. In order to get a better understanding of the $\mathbf{E}\times\mathbf{B}$ shear and its connection to the transition from L- to H-mode detailed measurements of E_r are highly desirable. The most commonly used tool to evaluate E_r is active charge exchange recombination spectroscopy (CXRS) [17]. At ASDEX Upgrade (AUG), a new high-resolution poloidal CXRS diagnostic utilizing one of the heating beams has been recently installed [18]. The measurements from this system, together with the data from the toroidal edge CXRS diagnostic [19, 18], enables the determination of E_r using the radial force balance equation, which holds locally for any plasma ion species α:

$$E_r = \frac{1}{n_\alpha Z_\alpha e}\frac{\partial p_\alpha}{\partial r} + v_{\perp,\alpha}B \tag{1}$$

$$= \frac{1}{n_\alpha Z_\alpha e}\frac{\partial p_\alpha}{\partial r} - v_{\theta,\alpha}B_\phi + v_{\phi,\alpha}B_\theta. \tag{2}$$

Here, n_α is the density, Z_α the charge state, e the elementary charge, $\frac{\partial p_\alpha}{\partial r}$ the radial pressure gradient of the species and $v_{\perp,\alpha}$ the species velocity perpendicular to the magnetic field B. Using the relation $\mathbf{e}_\perp = -\frac{B_\phi}{B}\mathbf{e}_\theta + \frac{B_\theta}{B}\mathbf{e}_\phi$, where $\mathbf{e}_\theta$ and $\mathbf{e}_\phi$ are the unit vectors in the poloidal and toroidal directions, equation (1) transforms to equation (2). Here, $v_{\theta,\alpha}$ and $v_{\phi,\alpha}$ correspond to the poloidal and toroidal rotation velocities of the species, while B_ϕ and B_θ denote the toroidal and poloidal magnetic field. The radial force balance relates the lowest-order flow ($v_{\theta,\alpha}$ and $v_{\phi,\alpha}$) on a magnetic surface to the local $\mathbf{E}\times\mathbf{B}$ velocity, i.e. the radial electric field, and to the diamagnetic flow (pressure gradient) [20].

The main advantage of deriving E_r from charge exchange (CX) measurements is the high accuracy in the spatial localization of the measurements. The measured active CX signal is localized in the volume where the lines of sight (LOS) of the CXRS diagnostics intersect the path of the neutral beam particles. Furthermore, a high-accuracy alignment with respect to the edge kinetic profiles is possible, because the temperature T_α of the ion species α is part of the CXRS measurements and thus, is rigidly connected to the E_r profile. Note that $T_\alpha \approx T_i$, T_i being the main ion temperature, since the energy equilibration time between impurities and main ions is short (several μs) compared to local transport time scales ($\sim$1 ms) (see appendix). Thus, this quantity is denoted as the ion temperature T_i throughout the paper.

The high temporal resolution of both edge CXRS diagnostics (2.2 ms) enables the study of the E_r profile during an ELM (edge-localized mode) [21] cycle. ELMs cause energy losses that lead to large heat and particle loads on the divertor targets, which are high enough to provoke damage and rapid erosion of these targets [22]. For ITER

the control or even the full suppression of ELMs is mandatory, while the pedestal top pressure, which affects the global energy confinement through stiff temperatures [23], should not be strongly reduced. One ELM mitigation technique is realized by applying non-axisymmetric magnetic perturbations (MPs) to the plasma edge [24, 25]. In this paper, the influence of MPs on the E_r profile is presented and the profile with and without the application of MPs is compared.

This paper reports on E_r profiles derived from CXRS measurements at the plasma edge of AUG. In section 2 a general description on the evaluation of E_r is provided. CXRS measurements on different impurity species allow the diagnostic technique to be validated and to test whether the E_r profile is consistently determined. The consistency check is presented in section 3 along with a comparison to Doppler reflectometry measurements. Section 4 discusses the interdependency of E_r and the main ion pressure gradient term. E_r profiles measured in different confinement regimes are presented in section 5 and a correlation between the depth of the E_r well and the pedestal top ion pressure and plasma energy confinement is discussed. The evolution of E_r during an ELM cycle is described in section 6. The effect of externally applied magnetic perturbations (with toroidal mode number $n = 2$) on the E_r profile is presented in section 7. Section 8 gives a summary of the findings and discusses the main results.

2. Derivation of E_r from CXRS measurements

For an accurate evaluation of E_r via the radial force balance equation (1), the poloidal and toroidal magnetic fields as well as temperature, density and poloidal and toroidal flow velocity of the observed species are required. The toroidal and poloidal magnetic field are determined from the equilibrium reconstruction of the plasma using CLISTE [26]. The edge CXRS diagnostics provide all of the remaining quantities [17] needed to evaluate E_r. The ion temperature is determined from the Doppler width, the rotation velocity from the Doppler shift and the impurity density from the spectral radiance of the active CX line. The observed spectral line is usually fitted with 2 Gaussians, one for the active CX component and one for the passive component [18, 27]. The following sign convention is used in this paper: ϕ is counter-clockwise viewed from above and θ points vertically downward at the outer midplane. Hence, poloidal rotation velocities, which are vertically upward at the low-field side, are negative (electron diamagnetic direction). In the standard magnetic configuration of AUG B_ϕ is negative and B_θ is positive. The plasma current, I_p, and the neutral beam injection (NBI) are pointing into the positive toroidal direction.

Figure 1 shows example temperature, density and rotation profiles of B^{5+} ($n = 7 \rightarrow 6$, $\lambda = 494.467$ nm) obtained with the edge CXRS diagnostics in a type-I ELMy H-mode with B_ϕ on-axis of -2.5 T, I_p of 1 MA, 5 MW of NBI, 0.8 MW of electron cyclotron resonance heating (ECRH) and a central line-averaged density of 8×10^{19} m^{-3}. Good agreement is obtained for the ion temperature and B^{5+} density profiles. The profiles are ELM-synchronized meaning that the data measured

during the occurrence of an ELM crash are excluded. Only measurements 2.2 ms before the onset of an ELM (which corresponds to the time resolution of the edge CXRS diagnostics) are selected if not stated otherwise. To obtain full edge profiles a radial plasma sweep [18] of 2 cm is performed during a time window of 800 ms. Note that the measurements in the scrape-off layer (highlighted in gray in figure 1) are omitted as in this region the impurity ion density along with the active CXRS signal drops rapidly and additional background emissions disturb the active spectra making active CXRS measurements unreliable.

To evaluate E_r each characteristic CXRS profile (T_i, n_α, $v_{\theta,\alpha}$ and $v_{\phi,\alpha}$) is fit with a spline function. The resulting fits are then used for the determination of E_r. Note that usually the T_i and n_α profiles measured by the toroidal system are used in the fitting procedure since the toroidal diagnostic has a higher radial resolution (3 mm [19] compared to 5 mm [18] for the poloidal system), which enables the gradients in the profiles to be determined to higher accuracy. In the considered discharge (#26598) data for $\rho_{pol} < 0.94$ from the poloidal system have also been used for fitting T_i and n_α.

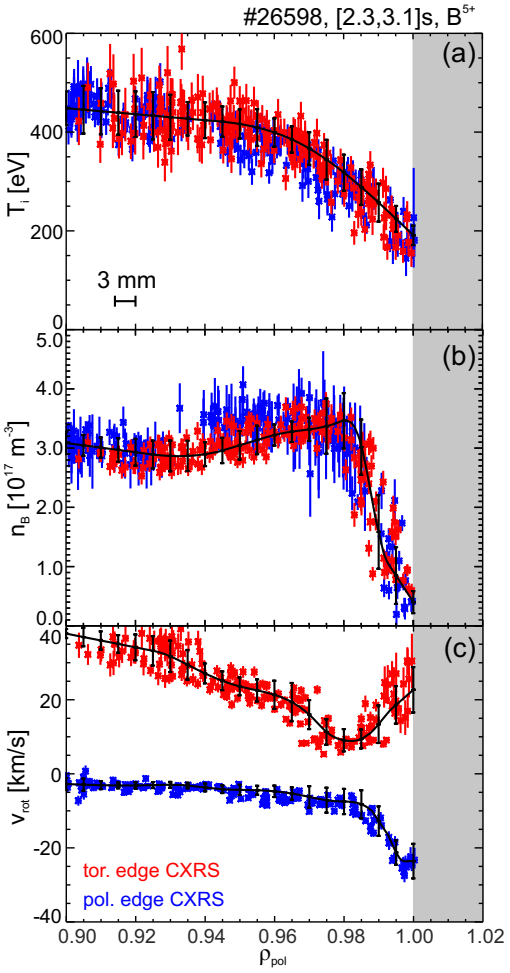

Figure 1: CX profiles obtained from measurements on B^{5+} in H-mode: (a) ion temperature, (b) B^{5+} density, (c) toroidal and poloidal rotation velocity.

In order to reduce uncertainties due to the magnetic equilibrium and to optimize the radial profile alignment [28] the following procedure is performed: the measurements obtained with the toroidal and poloidal system are aligned via the T_i and n_α profile. The relative alignment of the CXRS systems is of minor importance for the positioning of E_r, as in the plasma edge the evaluation of E_r is dominated by the poloidal impurity ion rotation contribution (see figure 2). While the radial resolutions of the diagnostics are 3 mm and 5 mm, respectively, the alignment is possible to a higher accuracy due to the steepness of the gradients, which are well resolved by the measurements. To align the CXRS profiles relative to the electron profiles it is assumed that the position of the steepest gradients in T_i coincide with those in the electron temperature, T_e, measured by the electron cyclotron emission (ECE) [29] and Thomson scattering (TS) [30] systems. While this assumption is not relying on fundamental physics, a highly reproducible radial alignment is found. The plasmas analyzed in the present work are in the collisionality

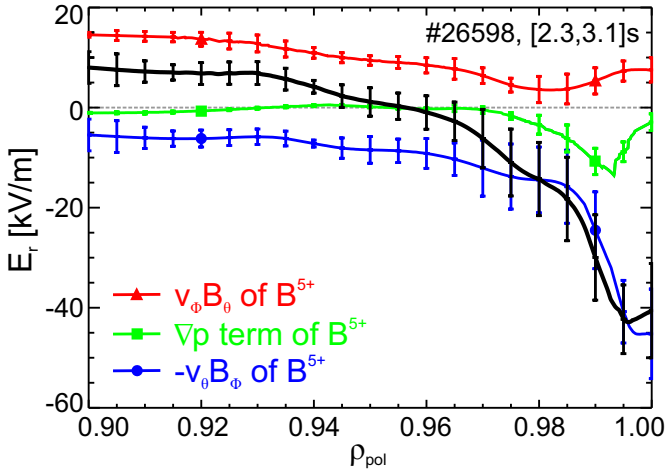

Figure 2: Radial electric field profile derived from CX measurements on B^{5+}: E_r in black, toroidal rotation contribution in red, pressure gradient term in green and poloidal rotation contribution in blue.

regime that is found to provide a sufficient coupling between the electrons and ions such that T_e is approximately T_i [31]. This is also supported by comparing the thermal equilibration times to the local transport time (see appendix). As the separatrix position is rigidly connected to the T_e profile via a power balance and parallel heat transport argument [32], also the relative alignment to the separatrix position is performed. To minimize the uncertainty of the separatrix position from the magnetic reconstruction, the required T_e value at the separatrix is ≈100 eV consistent with studies using a 1-D heat conduction model [32]. The T_i profile is then aligned relative to the T_e profile (and thus, relative to the separatrix) such that the steep gradient regions match each other. The accuracy of this relative profile alignment is estimated to 2 – 3 mm as T_e is closely connected to the separatrix position. The alignment of the profiles is simultaneously performed with respect to the electron density, n_e, profile as the TS system has identical measurement volumes for both n_e and T_e. The n_e measurements from TS are complemented by those obtained with the lithium beam (LIB) diagnostic [33, 34], which are shifted such that they match those of TS, and the interferometry system [35]. The latter is used to constrain the electron density at the pedestal top. The various diagnostics measure in different sectors of the tokamak vessel and the profiles are aligned radially assuming a toroidally symmetric equilibrium. Note that the shifts applied for the profiles are within the radial resolution of each diagnostic. This method enables the determination of the position of E_r relative to the electron profiles and to the separatrix position with an accuracy of 2 – 3 mm (indicated by a horizontal error bar in figure 1(a)).

Figure 2 shows the E_r profile deduced from the profiles of B^{5+} in figure 1 in black. In the ETB a negative E_r well, a narrow, localized minimum close to the separatrix, is found. Towards the plasma core, the magnitude of E_r decreases and changes sign (i.e. becomes positive). The error bars shown in figure 2 are calculated via Gaussian

error propagation using the standard deviation of the measured data in a small radial interval (± 0.005 in ρ_{pol}, which is of the order of the radial resolution of the diagnostics). In figure 2 the individual terms in the radial force balance equation (1) are colour-coded: the pressure gradient term (green), the toroidal rotation term (red) and the poloidal rotation term (blue). In the radial force balance of impurity ions the poloidal rotation term is the main contribution for the evaluation of the E_r well. Towards the plasma core E_r is dominated by the toroidal rotation velocity.

3. Validation of the E_r measurements

3.1. Comparison of different impurity ions

Performing CX measurements on different impurity species allows the validation of the diagnostics and a consistency check of E_r to be obtained since E_r must be the same for all impurities [36]. Thus, all analyses must arrive at the same E_r profile regardless of the impurity species used. For this purpose the discharge described in section 2 was repeated to obtain CX measurements on He^{2+} ($n = 4 \rightarrow 3$, $\lambda = 468.571$ nm) and C^{6+} ($n = 8 \rightarrow 7$, $\lambda = 529.059$ nm). The resulting E_r profiles are shown in figure 3(a). Within the uncertainties, good agreement between the three different impurity species is obtained, not only in the minimum of the E_r well, but also in the profile shape towards the plasma core. In a separate discharge a neon puff was included to cross-check the E_r profile with a fourth species. Due to the spectral range covered by the edge CXRS diagnostics (12.19 nm for the toroidal system and 7.84 nm for the poloidal system at a central wavelength of $\lambda = 527.5$ nm), simultaneous measurement of both C^{6+} and Ne^{10+} ($n = 11 \rightarrow 10$, $\lambda = 524.897$ nm) is possible. The resulting E_r profiles are shown in figure 3(b). The E_r profile is reproducible within the uncertainties regardless of the trace impurity used for the analysis.

For all impurity species analyzed in H-mode plasmas, the poloidal rotation

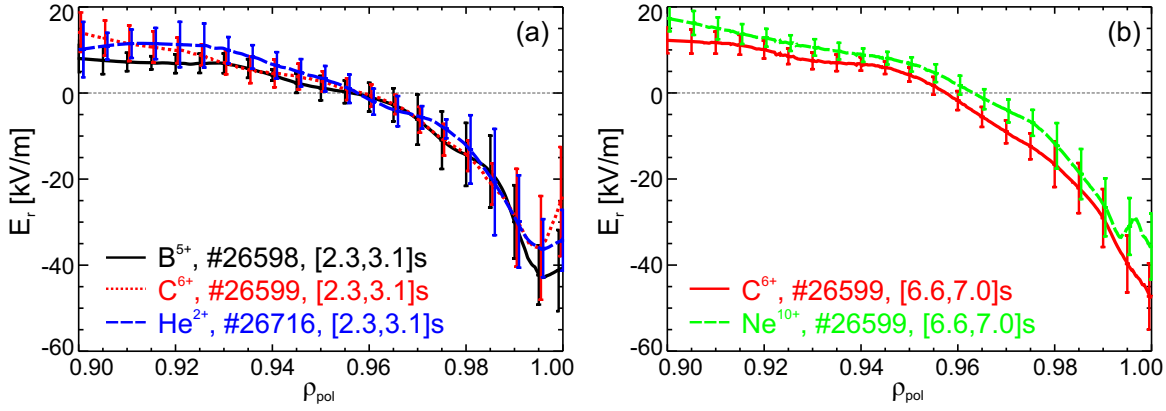

Figure 3: Radial electric field profile determined from CX measurements on different impurity species: (a) B^{5+} in black, C^{6+} in red (dotted line), He^{2+} in blue (dashed line), (b) C^{6+} in red and Ne^{10+} in green (dashed line) during the Ne-seeded phase.

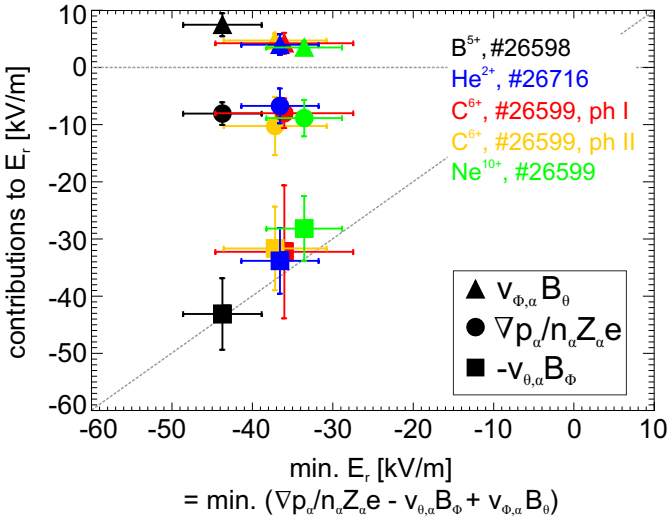

Figure 4: Individual impurity ion contributions for the evaluation of E_r versus minimum of E_r in H-mode: for impurity ions the poloidal rotation term is the main player in the evaluation of E_r. The label 'C^{6+}, #26599, ph I' corresponds to the non-seeded phase and 'C^{6+}, #26599, ph II' to the Ne-seeded phase.

contribution is dominant in the radial force balance. In figure 4 the individual impurity ion contributions at the radial position of the E_r minimum are plotted against the minimum of the E_r well. Note that for the Ne-seeded phase the C^{6+} contributions correspond to the position of the minimum of E_r derived from the Ne^{10+} measurements, as no clear minimum is visible for C^{6+}. For all impurities, the toroidal rotation term and the pressure gradient term have almost the same value in absolute magnitude and cancel each other, while the poloidal impurity ion rotation term is the dominant contribution for the evaluation of the depth of the E_r well. This also indicates that the poloidal rotation is at neoclassical levels [37, 38].

3.2. Comparison to Doppler reflectometry measurements

The E_r profile derived from the CXRS measurements has been compared to Doppler reflectometry (DR) measurements. In contrast to CXRS, which measures the impurity particle velocity and makes use of the radial force balance equation to evaluate E_r, the DR diagnostic measures the perpendicular fluid velocity of the electron density fluctuations which can be related to the local $\mathbf{E}\times\mathbf{B}$ velocity. The DR technique [39] is based on the backscattering of an oblique microwave beam with respect to the cut-off layer normal. The spectrum of the backscattered microwave is Doppler shifted by $\omega_D = \mathbf{u}\cdot\mathbf{k}$ and gives information on the velocity of the plasma fluctuations, $\mathbf{u}$, and on its wavenumber $\mathbf{k}$. By aligning the reflectometer perpendicular to the magnetic field such that the antenna is only sensitive to the perpendicular wavenumber, the Doppler shift results in $\omega_D = u_\perp k_\perp$, where $u_\perp$ is the perpendicular velocity of the electron density fluctuations and $k_\perp$ their perpendicular wavenumber. With knowledge of the

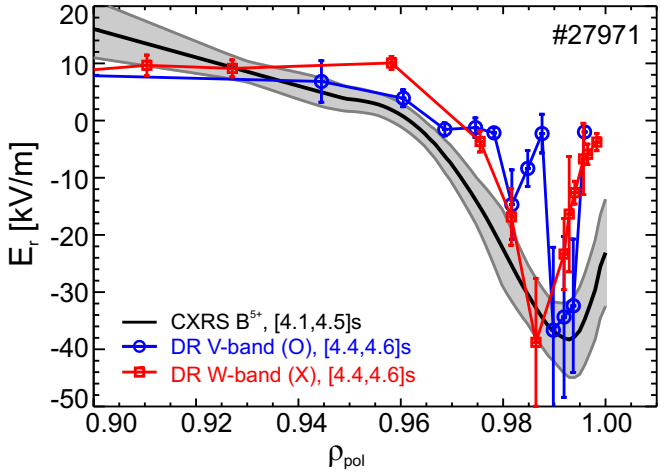

Figure 5: Radial electric field profile derived from CXRS and DR measurements.

perpendicular wavenumber, $u_\perp$ is determined directly from the measured Doppler shift ω_D. The perpendicular velocity corresponds to the sum of the $\mathbf{E}\times\mathbf{B}$ velocity of the plasma ($v_{\mathbf{E}\times\mathbf{B}}$) and the phase velocity of the density fluctuations (v_{ph}), $u_\perp = v_{\mathbf{E}\times\mathbf{B}} + v_{ph}$. Usually, v_{ph} is assumed to be negligible: an assumption that is supported by comparative measurements performed at multiple devices e.g. W7-AS [40], TJ-II [41], DIII-D [42] and AUG in the plasma core [4]. Hence, E_r is given by $E_r = u_\perp B$. At AUG two DR diagnostics are installed, a dual channel V-band ($50-75$ GHz) system [43] and a W-band ($75-110$ GHz) system [44, 45] with steppable launching frequencies (O-mode and X-mode polarization).

In order to compare the E_r profiles dedicated discharges have been conducted. The experiment presented was performed in H-mode with $B_\phi = -2.3$ T, $I_p = 0.8$ MA, 2.5 MW NBI, 1.7 MW ECRH and a central line-averaged density of 5.7×10^{19} m^{-3}. A radial plasma sweep was included to provide detailed edge CXRS profiles. The plasma density was regulated such that both Doppler systems could resolve the edge pedestal. Figure 5 shows the E_r profile derived from CXRS measurements on B^{5+} in black and the profile obtained with DR in blue (V-band, O-mode polarization) and red (W-band, X-mode polarization). While for the CXRS measurements the radial resolution is increased by performing a radial plasma sweep, the DR profiles result from frequency sweeps over a time period of 200 ms. During these sweeps the plasma was in a steady-state phase. Good agreement is found for the depth of the E_r well and its radial position is consistent within the uncertainties of the diagnostics. The differences in the width of the E_r well result in different levels of E_r shear and might be explained by the radial resolution of each system. While the DR diagnostics rely on the local density profile to determine the exact measurement location, the CXRS measurements are fixed in real space. In addition, the location of the DR measurements might be sensitive to fluctuations of the edge density profile, which could explain the non-monotonic appearance of the E_r profiles from DR (i.e. at $\rho_{pol} \sim 0.985$ E_r decreases to almost 0 and then increases again). These fluctuations might affect the propagation of the electromagnetic wave and thus,

the measurement location might be shifted from the actual position. Small changes in the local density profile can affect the radial localization of the E_r profile. The radial resolution of the DR systems depends on the density gradient, the frequency and the polarization. For the AUG DR diagnostics the radial resolution is of the order $\lesssim 0.01$ in ρ_{pol}, while for the edge CXRS systems it is approximately 0.006. Further comparative measurements are needed to quantify the difference in the E_r shear.

In the following the E_r profile derived from CXRS is presented in detail as it is intrinsically aligned to the T_i profile. The alignment to the kinetic electron profiles and to the separatrix position is performed straightforward, thus, enabling an accurate comparison to the gradients of the main ion species.

4. Comparison of E_r and the main ion pressure gradient term

The radial electric field is supposed to be driven by the main ions, typically deuterium at AUG, and not by the impurities. However, measurements of the main ion population using CXRS are difficult to interpret due to large background emissions and the beam halo [17]. Usually, CXRS measurements are performed on impurity ions as the diagnostic method is easily applicable. Since E_r is the same for every species, the profile derived from the impurity ions allows information on the main ion species to be obtained indirectly. For this purpose, an estimate of the pressure gradient term of deuterium is calculated using the assumption of quasi-neutrality and two assumptions on the ion density profile: (i) constant dilution, $n_i \propto n_e$ (n_i being the ion density and n_e the electron density), leading to

$$\frac{\nabla p_i}{n_i} = \frac{\nabla(n_i T_i)}{n_i} = \frac{C\nabla n_e}{C n_e} T_i + \nabla T_i = \frac{\nabla n_e}{n_e} T_i + \nabla T_i \tag{3}$$

and (ii) radially varying dilution with $n_i = n_e(1 - \sum_\alpha Z_\alpha c_\alpha)$, c_α being the radially dependent concentration of the impurity species α. The n_i profile has been calculated using the boron and carbon concentrations as measured with CXRS in subsequent discharges. The radial concentration of boron (carbon) changes from 0.2 % to 0.5 % (0.4 % to 0.6 %) over the pedestal region.

Figure 6(a) depicts the E_r profile in black obtained from CXRS on B^{5+}, while the pressure gradient term of deuterium is shown in red. Here, T_i is used from the CXRS measurement, while n_e is taken from measurements with TS, the LIB diagnostic and the interferometry system. Note that the T_i and n_e profiles have been aligned relative to each other as described in section 2. The modification of the main ion pressure gradient term due to a non-constant dilution (see blue dashed line in figure 6(a)) is found to be small (the maximum difference is less than 1.5 kV/m).

The pressure gradient term of deuterium is very similar to E_r indicating that for the main ions the pressure gradient term is the main contribution in the radial force balance. From this comparison an estimate of the perpendicular flow velocity of the

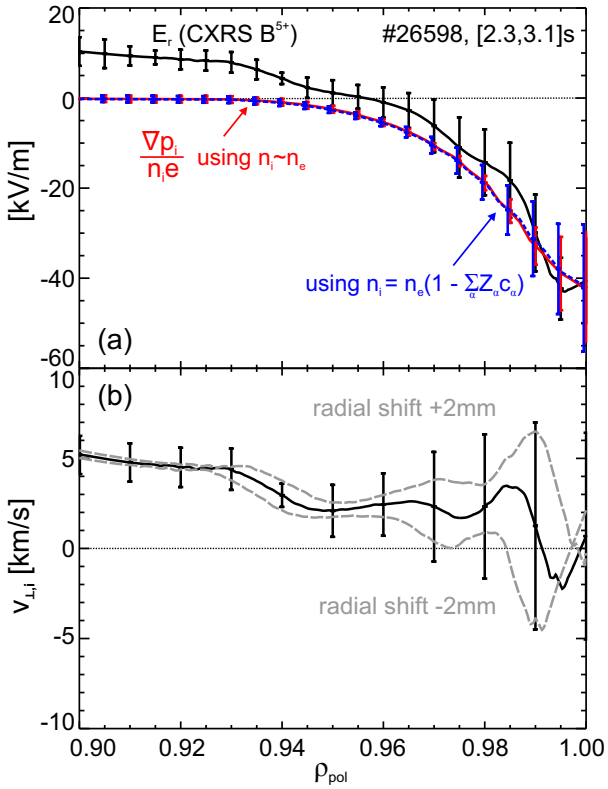

Figure 6: (a) Comparison of E_r (black curve) to an estimate of the main ion pressure gradient term assuming constant dilution (red curve) and correcting for the effect of impurities (blue dashed line), (b) derived perpendicular main ion velocity. The dashed lines in the lower panel show the effect of a relative shift between electron and ion profiles by ±2 mm.

main ions, $v_{\perp,i}$, can be calculated via a rearrangement of equation (1):

$$\Rightarrow v_{\perp,i} = \frac{1}{B}\left(E_r - \frac{1}{e}\left(\frac{\nabla n_i}{n_i}T_i + \nabla T_i\right)\right) \tag{4}$$

In figure 6(b) the calculated main ion flow velocity perpendicular to the magnetic field is shown. The perpendicular main ion flow is positive, i.e. in the ion diamagnetic drift direction. Note that $v_{\perp,i}$ is small in magnitude. Within an uncertainty of 5 km/s, it approaches $v_{\perp,i} = 0$ inside the ETB, similar to results obtained at Alcator C-Mod [6]. The dashed lines in figure 6(b) show the effect of a radial shift of ±2 mm between n_e and T_i measurements.

Helium plasmas provide the opportunity to obtain direct information on the main ion species by using CXRS on He^{2+}. These measurements have been performed in an H-mode discharge with $B_\phi = -2.5$ T, $I_p = 1.0$ MA, 0.5 MW ECRH, 9.2 MW deuterium NBI heating and a central line-averaged density of 1.1×10^{20} m^{-3}. At the plasma edge E_r is found to be dominated by the pressure gradient term of He^{2+} while the Lorentz force term is small and approaches zero close to the separatrix (see figure 7(a)). In the analysis the plume effect is not taken into account, however, the contribution of the

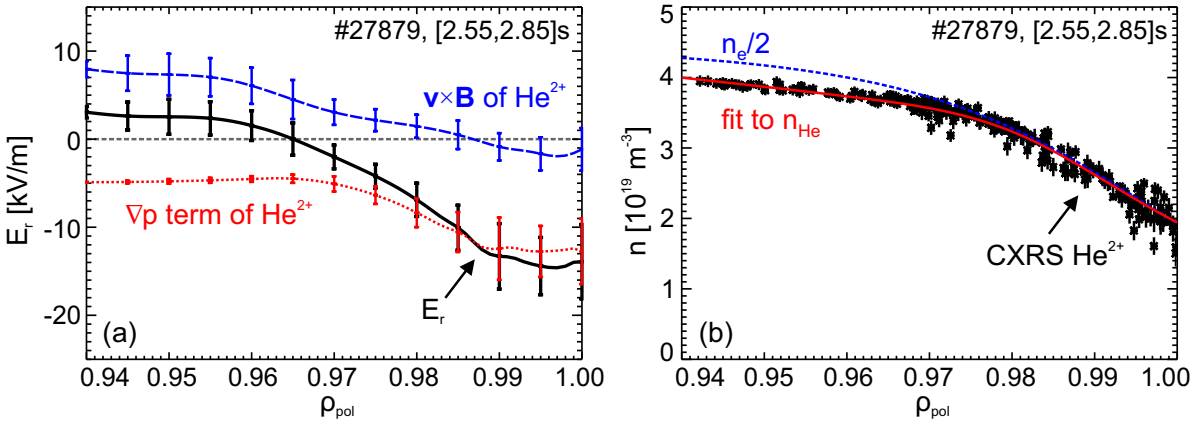

Figure 7: CXRS measurements in a helium plasma: (a) E_r profile in black, pressure gradient term of He^{2+} in red (dotted line) and $\mathbf{v} \times \mathbf{B}$ term of He^{2+} in blue (dashed line), (b) measured helium density profile in black, fit in red and fit to electron density profile in blue (dashed line). The fit to n_e is scaled by a factor of 2.

helium plume is expected to be small at the plasma edge [17]. This is also confirmed by independent density measurements using the LIB, TS and interferometry diagnostics: as expected, the helium density is found to be half the electron density and the gradients match, i.e. $\nabla n_i = \nabla n_e/2$. Figure 7(b) shows the measured helium density profile, along with a fit (red line) and a fit to the electron density profile (blue dashed line). The fit to n_e has been scaled by a factor of 2.

These results are in agreement with neoclassical theory [20] which predicts that to zeroth order, and in case of small toroidal rotation velocities, the edge radial electric field is balanced by the ion pressure gradient normalized to the ion density [46]. Quantitative comparisons between measurements and neoclassical codes are beyond the scope of this paper and will be presented in a subsequent publication. Investigations on this subject have been performed in [47], which concludes that in H-mode the depth of the edge radial electric field is well described by neoclassical theory.

5. E_r profiles in different confinement regimes

Previous work on several devices has demonstrated a connection between edge E_r profiles and global plasma energy confinement [48, 49, 50, 4, 6, 51]. This connection has also been examined in AUG discharges using the data from the new edge CXRS systems. In order to explore this over the widest range of plasma parameters possible, E_r profiles have been collected from many different types of discharges including L-, I-, H- and improved H-mode plasmas. Figure 8(a) shows the E_r profile obtained in an L-mode deuterium plasma with B_ϕ on axis of -2.5 T, I_p of 1 MA and 1 MW NBI heating. The CX measurements were performed on He^{2+}. In L-mode the radial electric field is small in magnitude and exhibits weak gradients. In this confinement regime both impurity ion velocity components are important for the evaluation of E_r, while the

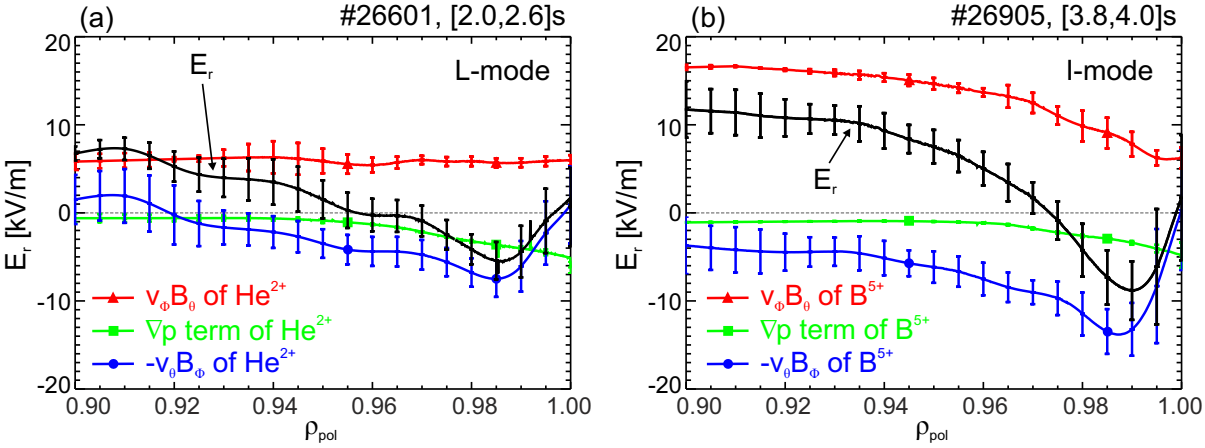

Figure 8: Radial electric field profile in (a) L-mode and (b) I-mode.

pressure gradient term of the impurity ion is almost negligible (cf. figure 8(a)). I-mode plasmas [52], originally referred to as 'improved L-mode' at ASDEX Upgrade [53], are characterized by similar energy confinement times as the H-mode, however, the particle confinement is near L-mode levels. In the I-mode regime (see figure 8(b)) the depth of the E_r well is found to be intermediate between L- and H-mode and dominated by the poloidal impurity ion rotation contribution. The radial electric field has also been studied in improved H-mode discharges with nitrogen (N_2) seeding. At AUG an improved confinement has been observed when using nitrogen as a low-Z radiator to protect the divertor [55]. In these plasmas the CX measurements are performed on a nitrogen line, i.e. N^{7+} ($n = 9 \rightarrow 8$) at $\lambda = 566.937$ nm. Figure 9(a) shows the resulting

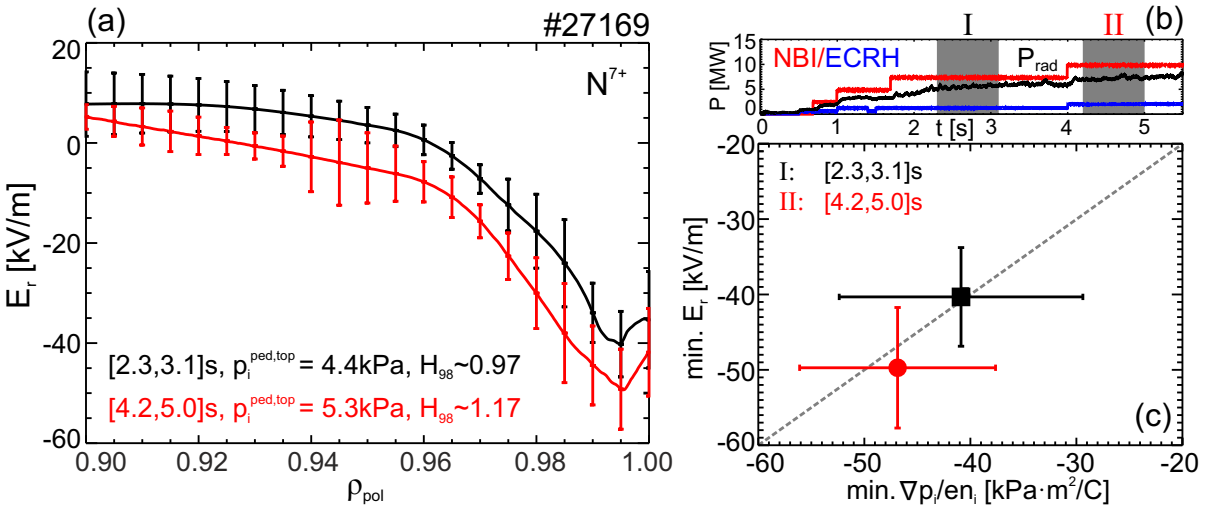

Figure 9: (a) Radial electric field profiles obtained in an improved H-mode discharge with different pedestal top ion pressures $p_i^{ped,top}$ (at $\rho_{pol} = 0.97$) and thus, different H/L scaling factors H_{98}(y,2) [54], (b) time trace of NBI, ECRH and radiation power (P_{rad}), (c) minimum of E_r versus minimum of main ion pressure gradient term.

E_r profiles obtained in two phases with different NBI and ECRH power. N_2 seeding was applied throughout the whole discharge and an increase in the pedestal top pressure is concomitant with an increase in the energy confinement (moving from phase I to phase II). The E_r well is observed to deepen with higher pedestal top pressures.

The effect of increasing the NBI heating was studied in the improved H-mode discharge and two different phases with 7.5 and 10 MW NBI (see figure 9(b)) were analyzed. Increasing the momentum has no observable effect on the relation between the radial electric field and the pressure gradient term of the main ions at the plasma edge (cf. figure 9(c)). Note that for the calculation of the main ion pressure gradient term, the dilution due to N_2-seeding was taken into account. This result supports that in H-mode E_r assumes a value such that the E_r well is in balance with the gradients in the main ion species and the perpendicular flow of the main ions vanishes at the plasma edge.

Combining the results obtained in L-, I-, H-mode and improved H-mode plasmas shows that the minimum of E_r is correlated with the ion pressure at the pedestal top $p_i^{ped,top}$ ($\rho_{pol} = 0.97$). Figure 10(a) shows the minimum of E_r as a function of $p_i^{ped,top}$. As the gradient of the edge pedestal pressure is strongly correlated with the value at the pedestal top [31], $p_i^{ped,top}$ is a good approximation of the ion pressure gradient at the E_r minimum. Data obtained in impurity seeded H-modes (including the improved H-mode discharge) are marked in gray in figure 10. A general trend is observed that for higher

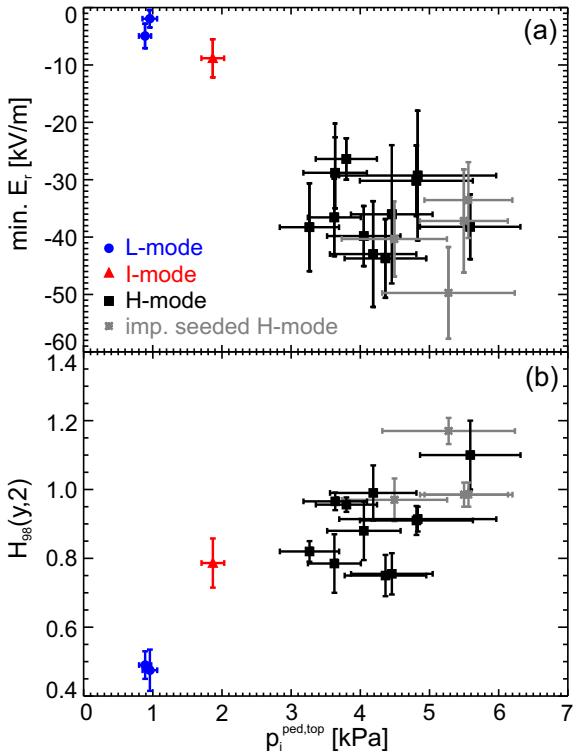

Figure 10: (a) Depth of E_r well as a function of pedestal top ion pressure $p_i^{ped,top}$ (at $\rho_{pol} = 0.97$), (b) energy confinement factor $H_{98}(y,2)$ versus $p_i^{ped,top}$.

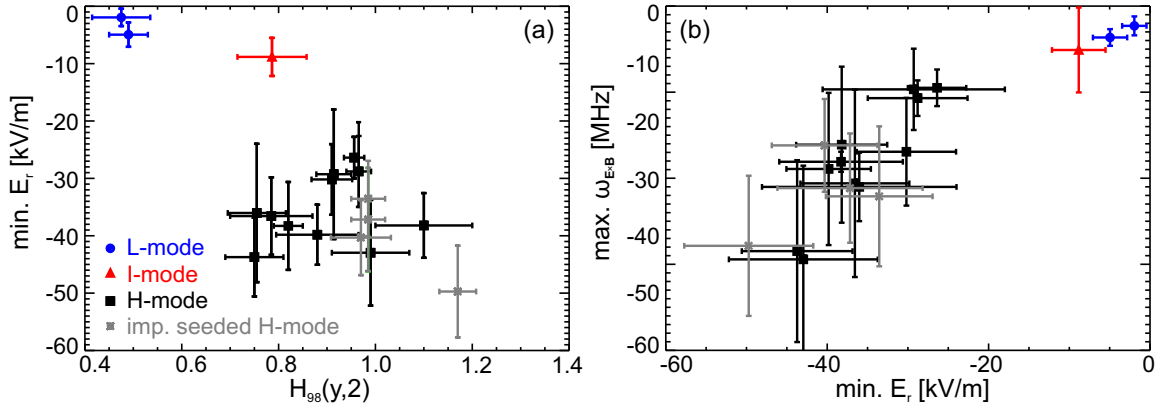

Figure 11: (a) Depth of E_r well as a function of the energy confinement factor $H_{98}(y,2)$, (b) maximum $\mathbf{E}\times\mathbf{B}$ shearing rate versus E_r minimum.

pedestal top pressures the E_r well is deeper, further confirming that E_r corresponds to the main ion pressure gradient term. Figure 10(b) shows the interdependence of the energy confinement factor $H_{98}(y,2)$ with respect to the ITER confinement scaling [54] and $p_i^{ped,top}$. The energy confinement increases for higher pedestal top ion pressures as a result of stiff T_i profiles. In figure 11(a) the minimum of E_r is plotted against the global energy confinement factor $H_{98}(y,2)$. Moving from L- to I- to H-mode the E_r well deepens and the energy confinement of the plasma increases. However, within the H-mode the scatter is substantial and no direct correlation between the depth of the E_r well and $H_{98}(y,2)$ is found. The observation of deep E_r wells at lower energy confinement factors ($\sim$0.75) is consistent with higher pedestal top pressures at lower $H_{98}(y,2)$ (cf. figure 10(b)). Since the maximum $\mathbf{E}\times\mathbf{B}$ shearing rate (defined as $\omega_{E\times B} = \frac{r}{q}\frac{\partial}{\partial r}(\frac{q}{r}\frac{E_r}{B})$ [56]) is strongly correlated to the E_r minimum (see figure 11(b)), $\omega_{E\times B}$ and the energy confinement factor have a similar relationship as the minimum of E_r and $H_{98}(y,2)$.

Within the framework of turbulence reduction theory through $\mathbf{E}\times\mathbf{B}$ shear [2], the following picture develops from these measurements: for constant E_r well widths [57, 6], deeper E_r wells have higher E_r shearing rates which increase the efficiency of turbulence reduction when moving from L- to H-mode. This leads to higher pedestal top pressures, which is correlated to the global plasma confinement. Hence, also the magnitude of the E_r shear is correlated to the energy confinement and increases from L- to H-mode [58]. Figure 12 shows (a) the E_r profiles and (b) the calculated E_r shear obtained in the different confinement regimes. In the L- and I-mode regime the shear is weak (smaller than in H-mode) and comparable to the width of the turbulence spectrum ($\sim$100 – 200 kHz at the plasma edge [59]), while in the ETB of the H-mode the E_r shearing rate reaches values of up to 3 MHz. It is worth noticing that in H-mode the maximum shear coincides with the maximum ion pressure gradient, ∇p_i (see figure 12(c)), calculated using the n_e profile, giving confidence that the radial alignment of the gradients and E_r is very accurate for the present work. Note also that the maximum in the E_r shearing rate, or alternatively the steepest ∇p_i, lies in the inner part of the E_r well, indicating

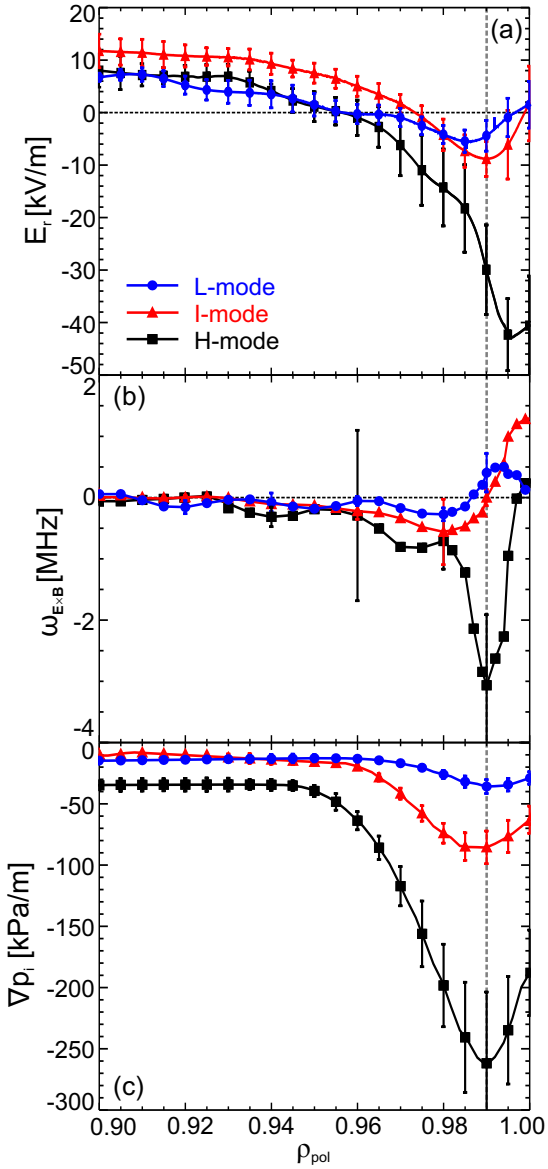

Figure 12: (a) E_r in L-, I- and H-mode and (b) resulting E_r shear. For better clarity the uncertainties are only shown for distinct radial positions. (c) Main ion pressure gradient, ∇p_i, in different confinement regimes.

that the negative shear region might be the important region for turbulence suppression consistent with previous results [60, 61, 4].
For the transition into H-mode it remains unclear whether there is a threshold of eddy size reduction leading to reduced turbulence and transport or a continual reduction of transport as the shearing rate increases.

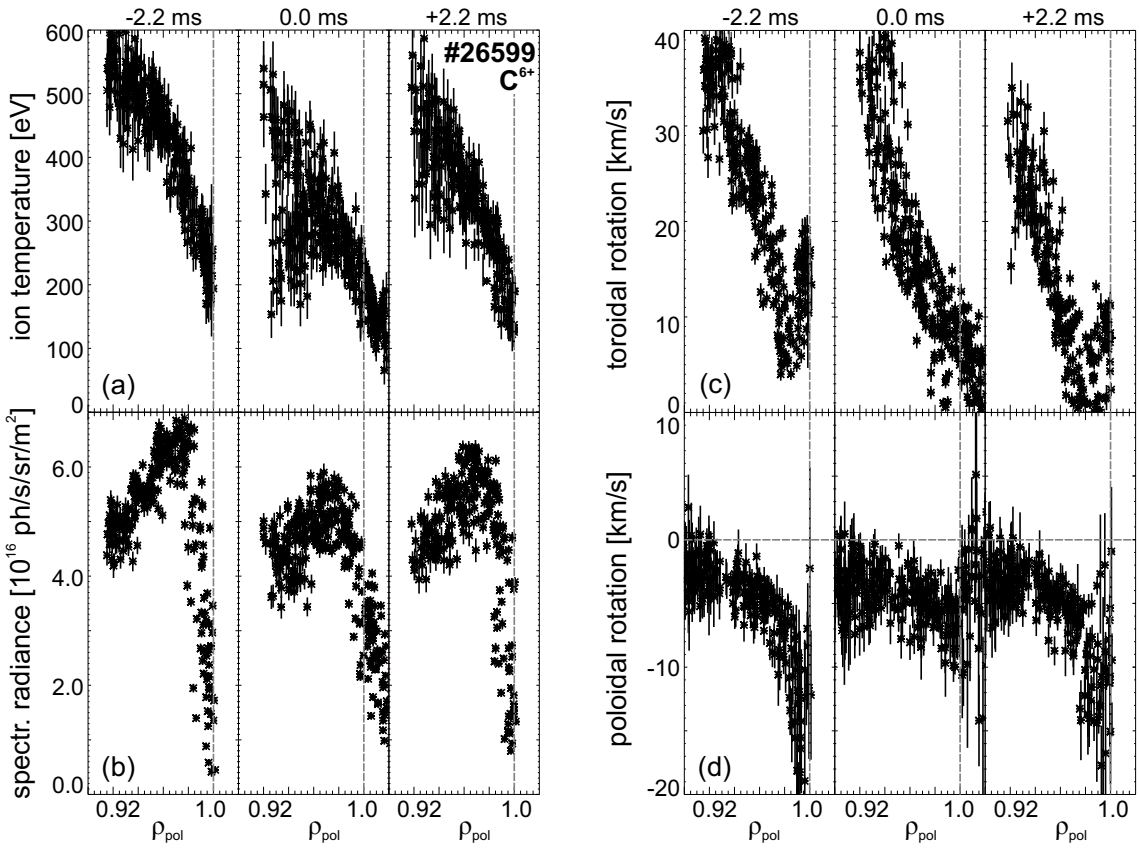

Figure 13: Evolution of CXRS measurements at different time points during an ELM cycle: (a) T_i, (b) spectral radiance of the active CX line, (c) toroidal rotation and (d) poloidal rotation. The labels '-2.2 ms', '0.0 ms' and '+2.2 ms' denote the relative time to the closest ELM. The profiles originate from a time window of 700 ms in which the plasma was radially moved through the views of the LOS. The vertical dashed line in each subfigure indicates the separatrix position.

6. Temporal evolution of E_r during an ELM cycle

Due to the occurrence of edge-localized modes (ELMs) the steep edge gradients of H-modes flatten transiently during each event. The temporal resolution of the edge CXRS diagnostics (2.2 ms) at AUG enables a synchronization of the data with respect to the onset of an ELM. Thus, the behaviour of the radial electric field during the ELM crash can be analyzed in detail. To this end, the data from a set of reproducible type-I ELM cycles measured in a time window of 700 ms, during which the plasma was radially moved through the views of the LOS to obtain complete edge profiles, has been sorted and mapped onto a time grid relative to the time of the closest ELM. The discharge is identical to the one discussed in section 2. The ELM frequency was constant at ∼80 Hz. Figure 13 shows the (a) T_i, (b) spectral radiance of the active CX line, (c) toroidal rotation and (d) poloidal rotation velocity profiles measured on C^{6+} during the ELM cycle. The labels '-2.2 ms', '0.0 ms' and '+2.2 ms' of figure 13 denote the relative time

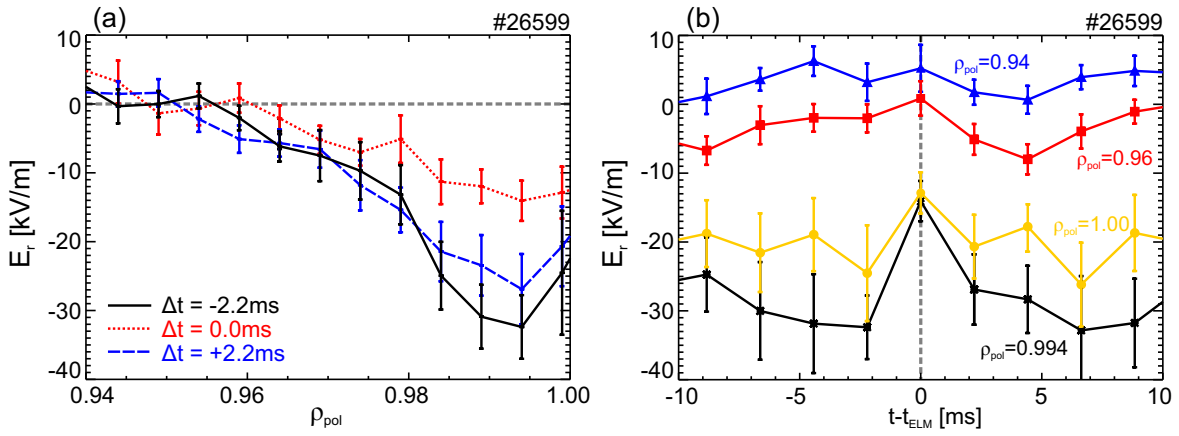

Figure 14: (a) Radial electric field profiles before, during and after an ELM, (b) E_r at distinct radial positions during an ELM cycle.

to the closest ELM at which the measurements were taken. Before the ELM T_i and the CX line intensity exhibit a strong gradient at the edge, while the toroidal rotation has a minimum localized at the pedestal top. The feature in the toroidal rotation profile has been reported in [19] and is further investigated in [37, 62]. The poloidal rotation on the other hand exhibits a local minimum close to the separatrix. During the ELM (labeled with '0.0 ms' in figure 13) the steep gradients flatten and the dips in both the toroidal and poloidal rotation vanish. Note that the integration time of the edge CXRS systems might be too long to quantitatively judge the behaviour of the impurity ion profiles, but the qualitative behaviour can be described. During the inter-ELM phase the signal in the scrape-off layer is not sufficient to analyze the CXRS spectral line, but when the ELM occurs the signal increases, indicating that the impurities are expelled, and the fits are trustworthy. The profiles start to recover and the typical pedestal structure is visible again already 2.2 ms after the ELM in agreement with experimental studies performed at DIII-D [63] and consistent with time scales of the electron profiles observed at AUG [64].

Figure 14(a) shows the resulting E_r profiles. The radial electric field is the deepest shortly before the ELM (black profile), while during the ELM crash the profile decreases in the ETB by up to a factor of 3 (red dotted profile), consistent with DR measurements [65]. The collapse of E_r results in a reduction of the E_r shear across the whole ETB. The destruction of the E_r shear layer at the ELM crash has also been observed in MAST using fast CXRS measurements with a time resolution of 200 μs [66]. Shortly after the ELM (+2.2 ms, blue dashed profile in figure 14(a)) the profile recovers and the E_r well reforms, reaching its initial depth 4 – 6 ms after the ELM event (cf. figure 14(b)), consistent with time scales observed at DIII-D [63]. Figure 14(b) shows the temporal evolution of E_r at different radial locations. Further inside the plasma E_r is almost not affected with only slight modifications during the ELM crash, while in the ETB the E_r well is strongly reduced. Note that the E_r well might even vanish for a brief time period that is too short to be detected by the diagnostics.

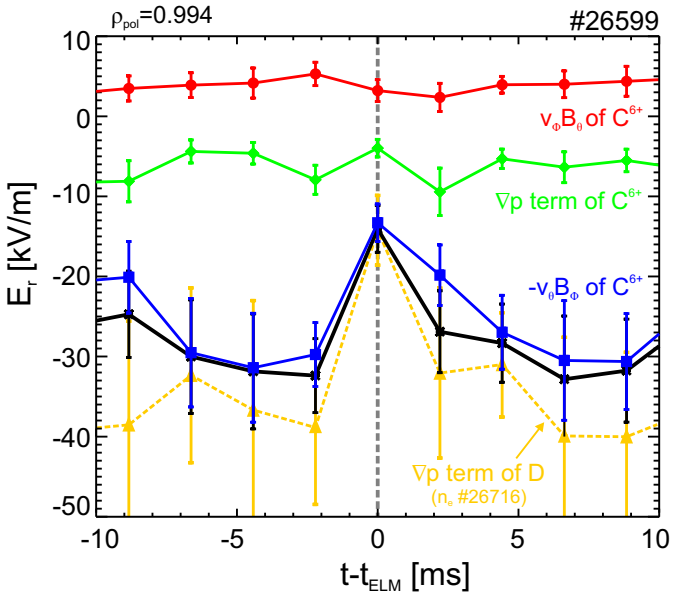

Figure 15: Individual impurity ion terms for the evaluation of E_r (red circles, green diamonds and blue squares) and main ion pressure gradient term (yellow triangles) at $\rho_{pol} = 0.994$ during an ELM cycle.

Figure 15 shows the contributions of the individual terms of the radial force balance equation to the E_r well during the ELM cycle. Throughout the entire ELM cycle the poloidal rotation term of the impurity ions is the dominant contribution for the evaluation of the E_r well. The temporal evolution of the main ion pressure gradient term is shown in yellow (triangles) in figure 15. The agreement in both the magnitude and evolution is remarkably good and shows that already ∼2 ms after the ELM crash both the p_i gradient and the E_r well are recovering. It should be noted that the main ion pressure gradient term has been calculated using the n_e profile from an identical discharge (#26716), as the edge n_e measurements were not available for the considered discharge.

7. Effect of magnetic perturbations on E_r

For the experimental campaign 2011, the AUG tokamak was equipped with the first set of in-vessel saddle coils which consisted of two rows of coils above and below the midplane [67]. Each row had four coils at different toroidal positions. The coils were used to apply non-axisymmetric magnetic perturbations (MPs) to the plasma in order to suppress type-I ELMs. In H-mode plasmas with externally applied MPs (toroidal mode number $n = 2$) ELM mitigation was observed above a critical edge density [68], corresponding typically to a fractional Greenwald density of $n_{e,ped}/n_{GW} \sim 0.65$, $n_{e,ped}$ being the pedestal electron density and n_{GW} the Greenwald density [69]. So far, ELM mitigation has been observed in plasmas with different shape, different heating mixes, different levels of heating power [70] and with MPs that are both resonant and non-

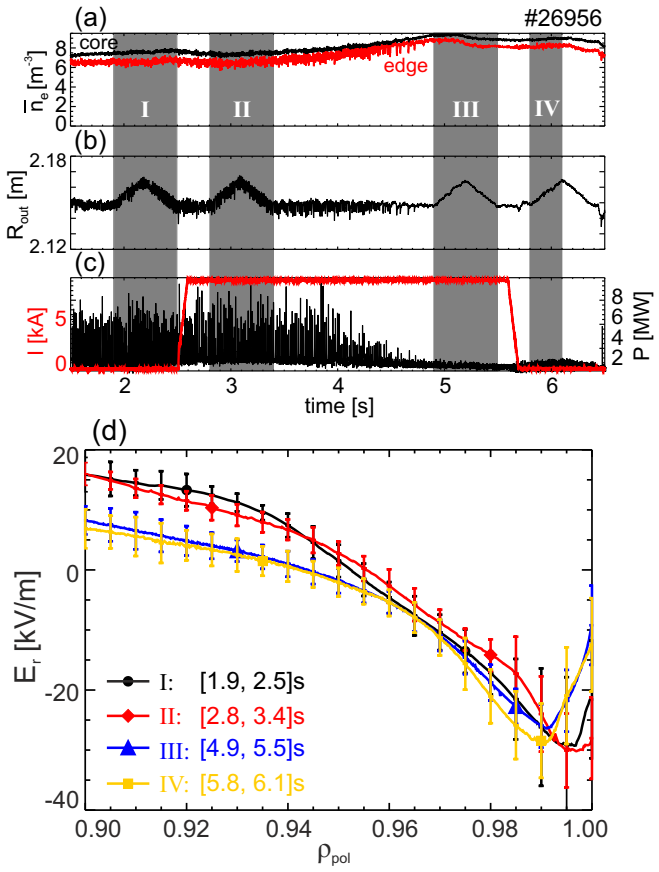

Figure 16: (a) Line-averaged density in the plasma core (black) and edge (red), (b) radial plasma position at outer midplane R_{out}, (c) ELM monitoring signal in the divertor (black) and current of MP coils (red), (d) radial electric field profiles corresponding to the different phases during the discharge (marked in gray in (a)-(c)). No obvious effect on E_r is observed due to the MP coils.

resonant with the edge q profile [68].

The experiment presented here was carried out specifically to test if there is an observable effect on the E_r profile due to the MPs. The discharge was designed with four phases (see figure 16), the first one without MPs, followed by a phase with MPs but without ELM mitigation. In the third phase (MPs on) the density was increased and ELM mitigation was achieved and in the last phase, the MPs were switched off. The discharge was performed in H-mode with $B_\phi = -2.4$ T, $I_p = 1$ MA, NBI heating of 7.6 MW and ECRH ranging between 1.5 and 2.2 MW. The safety factor at the surface that encloses 95% magnetic flux, q_{95}, was ranging between 4.05 and 4.35 throughout the different phases of the discharge. The $n = 2$, odd configuration (odd corresponding to the opposite parity of upper and lower MP coils) was used. Figure 16(a) shows the time trace of the line-averaged electron density from a central LOS and an edge LOS of the interferometry system. The radial plasma position at the outer midplane (see figure 16(b)) was scanned several times to obtain detailed edge profiles in each phase.

In figure 16(c) the current of the MP coils and an ELM-monitoring signal in the divertor are plotted. At a line-averaged edge density of 6.5×10^{19} m^{-3} the application of the MP coils has no effect on the ELMs. However, as soon as a critical edge density is achieved (cf. phase III) the type-I ELMs disappear. From the CXRS measurements in each radial sweep, E_r profiles were obtained by measuring the B^{5+} CX line (see figure 16(d)). For phase I and II the inter-ELM E_r profile is shown. In general, the E_r profile does not exhibit any significant change due to the MPs. Moving from phase I to II and switching on the MP coils has no effect on the ELMs and no change in E_r is observed. As the plasma density increases (moving from phase II to III) the type-I ELMs disappear. However, the E_r well (see blue curve of figure 16(d)) is not affected and stays constant also when the coils are switched off. Comparing the E_r profile of phases II and III, the minimum of the E_r well appears to be slightly shifted inwards. This shift corresponds to about 2 mm in real space and is just within the error bars. Towards the plasma core the radial electric field decreases by ∼8 kV/m (at $\rho_{pol} = 0.9$). Note that this reduction and the radial shift are mainly attributed to the increase in the gas puff level and hence, plasma density. In the last phase the density stays at the same level and the MP coils are switched off. Here, the type-I ELMs do not return, however, small high-frequent ELMs (∼200 Hz) appear. Note that the radial electric field shows again no response.

These results suggest that in the plasmas studied so far (H-modes at high density) the edge radial electric field is not affected by externally applied MPs. The fact that E_r remains unaffected may be explained by the shielding of the plasma, i.e. the MP is not fully penetrating into the pedestal. Similar observations were reported from DIII-D in H-mode plasmas with resonant MPs in the $n = 3$ configuration with odd parity and $q_{95} = 3.8$ [71]. Here, the E_r minimum remained unchanged while in the scrape-off layer E_r increased. At TEXTOR an effect of resonant MPs on E_r has been observed [72], resulting in a maximum increase of E_r by 9 kV/m with respect to a reference discharge without MPs. This is attributed to the penetration of open field lines into the confined plasma. Preliminary AUG results in low density L-mode plasmas [73] show that the edge radial electric field is affected by the MPs, i.e. the E_r well is reduced.

In the 2011 opening, the installation of the in-vessel saddle coils system at AUG was completed, thus enabling operation with MPs up to n=4. Further experiments will be performed to study the effect of the MPs from the completed set of coils on the E_r profile.

8. Discussion and Summary

Extending the AUG edge CXRS system with a poloidal view enabled the determination of E_r from CX measurements using the radial force balance equation for impurity ions. The edge E_r profile is derived from CX measurements on He^{2+}, B^{5+}, C^{6+} and Ne^{10+} and is found to be identical within the uncertainties regardless of the impurity species used for the analysis. This demonstrates the validity of the diagnostic technique and provides a consistency check of E_r. In the radial force balance of impurity ions, the

poloidal rotation term is the dominant contribution for the evaluation of the E_r well consistent with measurements on other tokamaks. However, for the main ions, which are supposed to drive E_r, the pressure gradient term is the dominant contribution in the edge transport barrier (ETB). An estimate of the perpendicular deuterium velocity has been calculated using the main ion pressure gradient term and the E_r profile derived from CXRS. For $\rho_{pol} > 0.95$, i.e. the pedestal, the results suggest that $v_{\perp,i}$ is 0 with uncertainties less than 5 km/s, in agreement with observations on Alcator C-Mod [6]. This is confirmed by direct measurements of the main ion temperature, density and rotation velocities in helium plasmas, which show that at the plasma edge E_r is determined by the pressure gradient term of the main ions. These results support that the E_r well behaves as expected from neoclassical theory.

The E_r profile has been measured in different confinement regimes. In L-mode, E_r is small in magnitude and exhibits little shear, while in the ETB of the H-mode a strong, negative E_r well and a localized minimum close to the separatrix ($\rho_{pol} > 0.99$) is found, consistent with observations in other fusion devices. The steepest gradients of the ion and electron profiles, i.e. the pedestal, are in the inner, negative shear region of the E_r well. In I-mode plasmas, the minimum of the E_r well is intermediate between L- and H-mode. A correlation between the depth of the E_r well, or the magnitude of the E_r shear respectively, and the ion pressure at the pedestal top is observed, in keeping with the main ion pressure gradient term being the dominant contribution to E_r.

The time resolution of the edge CXRS diagnostics (2.2 ms) allows the study of the temporal evolution of E_r during an ELM cycle. At the ELM crash the E_r minimum decreases leading to a reduction of the $\mathbf{E}\times\mathbf{B}$ shear layer. Shortly after the ELM, the profile recovers and the E_r well reforms reaching its initial value 4 – 6 ms after the ELM. A comparison to the main ion pressure gradient term suggests that the ion pressure gradient and the E_r well recover on similar time scales.

In high density type-I ELM-mitigated H-mode plasmas, obtained via externally applied magnetic perturbations with toroidal mode number $n = 2$, no obvious effect on the E_r profile is visible.

The CXRS data presented in this paper are consistent with reductions in energy transport due to the suppression of turbulence. However, the self-consistent evolution of the E_r profile, pedestal shape, edge turbulence and transport reduction and improvement in plasma confinement is not completely elucidated due to the lack of clear definition of our understanding. The fact that the maximum $\mathbf{E}\times\mathbf{B}$ shearing rate coincides with the steepest ion pressure gradient and is localized in the inner part of the E_r well suggests that the negative shear region might be the important region for turbulence reduction within the $\mathbf{E}\times\mathbf{B}$ shear model [2]. The results discussed in this paper underline that the ion channel plays a key role in the interdependency between $\mathbf{E}\times\mathbf{B}$ shearing, turbulence and transport reduction.

9. Acknowledgments

The first author would like to thank E. Fable and U. Stroth for very fruitful discussions. M. Willensdorfer is a fellow of the Friedrich Schiedel Foundation for Energy Technology.

Appendix

In order to justify the approximation of $T_i \approx T_\alpha$, the equilibration times are compared to typical transport time scales at the plasma edge. Here, the particle transport time is defined as $\tau_{tr} = L_{n_e}^2/D$, where L_{n_e} is the electron density scale length and D the local diffusion coefficient. The thermal equilibration time between two different species is determined using the definition in [74]:

$$\tau_{\alpha\beta} = \frac{1}{1.8 \times 10^{-19}} \frac{(m_\alpha T_\beta + m_\beta T_\alpha)^{3/2}}{\sqrt{m_\alpha m_\beta}(Z_\alpha Z_\beta)^2 n_\beta \ln\Lambda} \tag{.1}$$

where m_α, m_β are the masses in g, T_α, T_β the temperatures in eV and Z_α, Z_β the charge states of the particle species α and β, n_β is the density of species β in cm^{-3} and lnΛ the Coulomb logarithm.

Figure 1 shows the local transport time scales in black for different diffusion coefficients (D = 0.1 m^2/s (dashed dotted line), D = 0.2 m^2/s (solid line) and D = 1 m^2/s (dashed line)). The values for the diffusion coefficients are taken from [75]. The thermal equilibration time between electrons and ions, τ_{ei}, is shown in red, while the time needed for a B^{5+} impurity to thermally equilibrate to the electrons, $\tau_{\alpha e}$, and to the main ions (deuterium), $\tau_{\alpha i}$, is shown in blue and green. At the plasma edge, the equilibration time

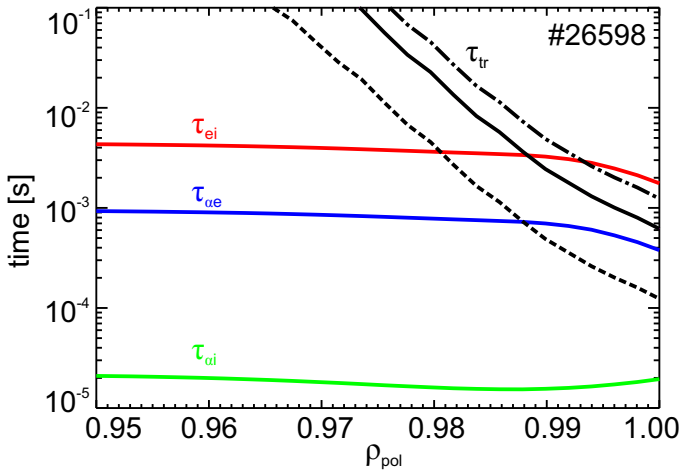

Figure 1: Typical time scales at the plasma edge of an H-mode discharge: transport time τ_{tr} in black, thermal equilibration time between electrons and ions (τ_{ei}) in red, between B^{5+} and electrons ($\tau_{\alpha e}$) in blue and B^{5+} and ions ($\tau_{\alpha i}$) in green. The local transport time scales have been evaluated using different diffusion coefficients (D = 0.1 m^2/s (dashed dotted line), D = 0.2 m^2/s (solid line) and D = 1 m^2/s (dashed line)).

between impurities and main ions is much shorter than the local transport time scale and thus, $T_i \approx T_\alpha$. The thermal equilibration time between impurities and electrons and electrons and ions is also faster than the local particle transport time. Only at the very plasma edge, close to the separatrix, the ions and electrons can decouple resulting in different ion and electron temperatures (with T_i usually being larger near the separatrix). Depending on the diffusion coefficient, also the impurities and electrons can decouple close to the separatrix. However, even in case of decoupling at the very edge, it is assumed that the position of the steepest gradients in T_i and T_e is the same since the transport barrier is build up in both the ion and electron channels.

References

[1] F. Wagner *et al.* *Phys. Rev. Lett.*, 49(19):1408, 1982.
[2] H. Biglari *et al.* *Phys. Fluids B*, 2(1):1, 1990.
[3] H. Meister *et al.* *Nucl. Fusion*, 41(11):1633, 2001.
[4] J. Schirmer *et al.* *Nucl. Fusion*, 46:S780–S791, 2006.
[5] K. H. Burrell *et al.* *Plasma Phys. Control. Fusion*, 31:10, 1989.
[6] R. M. McDermott *et al.* *Phys. Plasmas*, 16:056103, 2009.
[7] Y. Andrew *et al.* *Eur. Phys. Lett.*, 83:15003, 2008.
[8] K. Kamiya *et al.* *Nucl. Fusion*, 51:053009, 2011.
[9] R. E. Bell *et al.* *Phys. Rev. Lett.*, 81(7):1429, 1998.
[10] J. W. Coenen *et al.* *J. Phys. B: At. Mol. Opt. Phys.*, 43:144015, 2010.
[11] H. Meyer *et al.* *Jour. of Phys.: Conference Series*, 123:012005, 2008.
[12] R. E. Bell *et al.* *Phys. Plasmas*, 17:082507, 2010.
[13] K. Ida *et al.* *Rev. Sci. Instrum.*, 71(6):2360, 2000.
[14] R. Brakel *et al.* *Plasma Phys. Control. Fusion*, 39:B273–B286, 1997.
[15] T. Happel *et al.* *Phys. Plasmas*, 18:102302, 2011.
[16] V. Antoni *et al.* *Phys. Rev. Lett.*, 79:24, 1997.
[17] R. J. Fonck *et al.* *Phys. Rev. A*, 29(6):3288, 1984.
[18] E. Viezzer *et al.* *Rev. Sci. Instrum.*, 83:103501, 2012.
[19] T. Pütterich *et al.* *Phys. Rev. Lett.*, 102(025001), 2009.
[20] F. L. Hinton and R. D. Hazeltine. *Rev. Mod. Physics*, 48(2), 1976.
[21] H. Zohm. *Plasma Phys. Control. Fusion*, 38(2):105, 1996.
[22] G. Federici *et al.* *Plasma Phys. Control. Fusion*, 45:1523, 2003.
[23] F. Ryter *et al.* *Plasma Phys. Control. Fusion*, 43(A323), 2001.
[24] T. C. Hender *et al.* *Nucl. Fusion*, 32:2091, 1992.
[25] T. E. Evans *et al.* *Phys. Rev. Lett.*, 92:235003, 2004.
[26] W. Schneider *et al.* *Fusion Engineering and Design*, 48:127, 2000.
[27] E. Viezzer *et al.* *Plasma Phys. Control. Fusion*, 53:035002, 2011.
[28] E. Wolfrum *et al.* *Fusion Energy 2008 (Proc. 22nd Int. Conf. Geneva, Switzerland, 2008) (Vienna: IAEA) CD-ROM file EX/P3-7,* `http://www-naweb.iaea.org/napc/physics/FEC/FEC2008/html/index.htm`.
[29] W. Suttrop. *Practical Limitations to Plasma Edge Electron Temperature Measurements by Radiometry of Electron Cyclotron Emission.* IPP Report 1/306, Max-Planck-Institute for Plasma Physics, Garching, Germany, 1997.
[30] B. Kurzan *et al.* *Rev. Sci. Instrum.*, 82:103501, 2011.
[31] P. A. Schneider *et al.* Analysis of Temperature and Density Pedestal in a Multi-machine Database. *submitted to Nucl. Fusion (January 2013).*
[32] J. Neuhauser *et al.* *Plasma Phys. Control. Fusion*, 44:855, 2002.

[33] R. Fischer *et al.* *Plasma Phys. Control. Fusion*, 50:085009, 2008.
[34] M. Willensdorfer *et al.* *Rev. Sci. Instrum.*, 83:023501, 2012.
[35] A. Mlynek *et al.* *Rev. Sci. Instrum.*, 81:033507, 2010.
[36] J. Kim *et al.* *Phys. Rev. Lett.*, 72(14):2199, 1994.
[37] K. D. Marr *et al.* *Plasma Phys. Control. Fusion*, 52(055010), 2010.
[38] G. Kagan *et al.* *Plasma Phys. Control. Fusion*, 53(025008), 2011.
[39] M. Hirsch *et al.* *Plasma Phys. Control. Fusion*, 43:1641, 2001.
[40] M. Hirsch *et al.* *Plasma Phys. Control. Fusion*, 48:S155, 2006.
[41] T. Estrada *et al.* *Plasma Phys. Control. Fusion*, 51:124015, 2009.
[42] G. R. McKee *et al.* *Phys. Plasmas*, 7:1870, 2000.
[43] G. D. Conway *et al.* *Plasma Phys. Control. Fusion*, 46:951, 2004.
[44] C. Tröster. *Development of a flexible Doppler reflectometry system and its application to turbulence characterization in the ASDEX Upgrade tokamak*. PhD thesis, Ludwig-Maximilians-Universität München, 2008.
[45] T. Happel *et al.* Design of a New Doppler Reflectometer Frontend for the ASDEX Upgrade Tokamak. *Proc. 10th International Reflectometry Workshop, http://www.igi.cnr.it/irw10/proceedings/HappelT.pdf*, 2011.
[46] U. Stroth *et al.* *Plasma Phys. Control. Fusion*, 53:024006, 2011.
[47] B. Wieland. *Investigations on radial electric fields in the edge transport barrier of H-mode discharges*. PhD thesis, Technische Universität München, 2011.
[48] K. Itoh and S.-I. Itoh. *Plasma Phys. Control. Fusion*, 38:1, 1996.
[49] K. H. Burrell. *Phys. Plasmas*, 4(5):1499, 1997.
[50] K. Ida. *Plasma Phys. Control. Fusion*, 40:1429, 1998.
[51] G. D. Conway *et al.* *Fusion Energy 2010 (Proc. 23rd Int. Conf. Daejeon, Republic of Korea, 2010) (Vienna: IAEA) CD-ROM file EX/1-1, http://www-naweb.iaea.org/napc/physics/FEC/FEC2010/index.htm*.
[52] D. G. Whyte *et al.* *Nucl. Fusion*, 50(105005), 2010.
[53] F. Ryter *et al.* *Plasma Phys. Control. Fusion*, 40:725, 1998.
[54] ITER Physics Expert Group on Confinement and Transport and Confinement Modelling and Database, ITER Physics Basis Editors. *Nucl. Fusion*, 39:2175, 1999.
[55] O. Gruber *et al.* *Nucl. Fusion*, 49(115014), 2009.
[56] T. S. Hahm and K. H. Burrell. *Phys. Plasmas*, 2(5):1648, 1995.
[57] P. Gohil *et al.* *Nucl. Fusion*, 38(1):93, 1998.
[58] P. Sauter *et al.* *Nucl. Fusion*, 52:012001, 2012.
[59] G. D. Conway *et al.* *Plasma Phys. Control. Fusion*, 44:451, 2002.
[60] R. A. Moyer *et al.* *Phys. Plasmas*, 2(6):2397, 1995.
[61] K. H. Burrell *et al.* *Phys. Plasmas*, 6(12):4418, 1999.
[62] T. Pütterich *et al.* *Nucl. Fusion*, 52:083013, 2012.
[63] M. R. Wade *et al.* *Phys. Plasmas*, 12:056120, 2005.
[64] A. Burckhart *et al.* *Plasma Phys. Control. Fusion*, 52:105010, 2010.
[65] G. D. Conway *et al.* *Plasma Fus. Research*, 5(S2005), 2010.
[66] H. Meyer *et al.* *Nucl. Fusion*, 51(113011), 2011.
[67] W. Suttrop *et al.* *Fusion Eng. Design*, 84(290), 2009.
[68] W. Suttrop *et al.* *Phys. Rev. Lett.*, 106(225004), 2011.
[69] M. Greenwald *et al.* *Nucl. Fusion*, 28:2199, 1988.
[70] W. Suttrop *et al.* *Plasma Phys. Control. Fusion*, 53:124014, 2011.
[71] R. A. Moyer *et al.* *Phys. Plasmas*, 12:056119, 2005.
[72] J. W. Coenen *et al.* *Nucl. Fusion*, 51(063030), 2011.
[73] M. Kočan *et al.* Far-reaching Impact of Intermittent Transport across the Scrape-off Layer: Latest Results from ASDEX Upgrade. *submitted to Nucl. Fusion (January 2013)*.
[74] J. D. Huba. *NRL Plasma Formulary*. Naval Research Laboratory, available at `http://wwwppd.`

`nrl.navy.mil/nrlformulary/`, 2007.
[75] T. Pütterich *et al. J. Nucl. Mater.*, 415(1):S334–S339, 2011.